Click Here for Full Article

Empirical modeling of light availability in rivers

J. P. Julian,[1,2] M. W. Doyle,[1] and E. H. Stanley[3]

Received 24 September 2007; revised 27 March 2008; accepted 3 April 2008; published 16 August 2008.

[1] While the influence of hydrology and geomorphology on ecosystem-limiting factors in rivers has been well studied, particularly habitat availability and nutrient cycling, the more fundamental limitation of light availability has received much less attention. Characterizing light regimes in rivers is optically complex and requires consideration of five hydrogeomorphic controls: topography, riparian vegetation, channel geometry, optical water quality, and hydrologic regime. To generalize and quantify these hydrogeomorphic controls, we developed an empirical model that predicts both spatial and temporal variability of photosynthetically active radiation reaching the riverbed (benthic PAR). We applied this benthic light availability model (BLAM) to two dissimilar systems: a large, turbid river and a small, optically clear river. Comparisons between the two systems revealed that the dominant control on temporal light availability for the large river was discharge, which accounted for 90% of the variation. A dominant temporal control for the small river did not emerge, but instead was found to be a function of both above-canopy PAR and discharge. Spatially, water depth accounted for 99% of the variation in benthic PAR for the large river, and riparian shading accounted for 93% of the variation for the small river. Channel orientation also had a major influence, where an E-W configuration increased benthic PAR by as much as 108% relative to a N-S configuration. BLAM predictions agreed well with measured benthic PAR, within 39% on average over a 9-d period. BLAM is the first model to quantify benthic PAR using all five hydrogeomorphic controls, and thus provides a new tool for investigating the role of light in fluvial ecosystem dynamics and for establishing light availability targets in water resource management.

Citation: Julian, J. P., M. W. Doyle, and E. H. Stanley (2008), Empirical modeling of light availability in rivers, *J. Geophys. Res.*, *113*, G03022, doi:10.1029/2007JG000601.

1. Introduction

[2] Many fundamental processes of aquatic ecosystems are driven by light availability, including photosynthesis, photochemical reactions, thermal fluctuations, and animal behaviors [*Wetzel*, 2001]. While the influences of hydrology and geomorphology on other ecosystem-limiting factors are increasingly studied (e.g., nutrient cycling, habitat [*Doyle and Stanley*, 2006; *Strayer et al.*, 2006]), the more fundamental limitation of light availability has received considerably less attention. Light studies in rivers may have been largely neglected because (1) of greater attention to nutrients in controlling primary production, (2) boundary conditions (banks, riparian vegetation) make ambient light measurements challenging, and (3) riverine optical water quality is highly variable and difficult to characterize [*Davies-Colley et al.*, 2003]. The little information that is available on riverine light regimes is derived mostly from New Zealand rivers under predominantly baseflow conditions, limiting current understanding of the temporal and spatial availability of light in rivers.

[3] Most of our knowledge on aquatic optics is derived from studies in oceans [*Jerlov*, 1976; *Mobley*, 1994] and lakes [*Kirk*, 1994; *Wetzel*, 2001]. These studies have shown that once light enters water it is attenuated exponentially with depth at a predictable rate depending on the type and quantity of water constituents [*Kirk*, 1994]. Light availability in rivers is optically more complex [*Davies-Colley et al.*, 2003; *Westlake*, 1966], requiring consideration of channel hydrology and geomorphology among other factors.

[4] Characterizing the light environment in rivers requires information on the surrounding topography, riparian vegetation, channel geometry, optical water quality, and hydrologic regime (Figure 1). These components, hereafter referred to as hydrogeomorphic controls, are primarily shaped by the river basin's climate and geology. Topography, including mountains, canyon walls, and riverbanks, affects light availability as an opaque barrier between solar irradiance and the river. Riparian vegetation also shades the water surface, but is not opaque. The percentage of light that riparian vegetation attenuates depends on the direction and intensity of above-canopy irradiance and the canopy struc-

[1]Department of Geography, University of North Carolina, Chapel Hill, North Carolina, USA.
[2]Now at Department of Geography, University of Oklahoma, Norman, Oklahoma, USA.
[3]Center for Limnology, University of Wisconsin, Madison, Wisconsin, USA.

Copyright 2008 by the American Geophysical Union.
0148-0227/08/2007JG000601$09.00

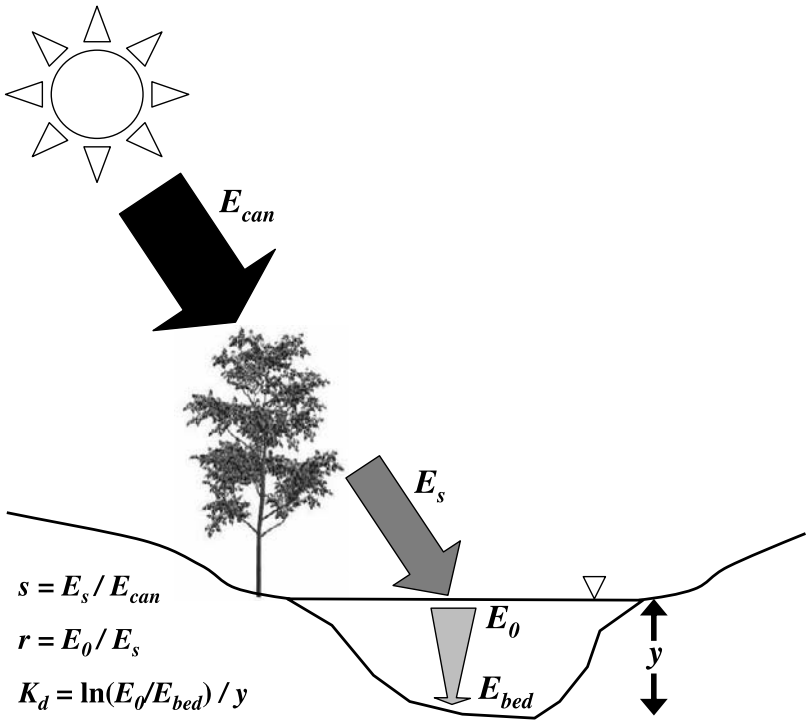

Figure 1. Light availability in rivers. E_{can} is the total solar irradiance available to the river before any shading from topography and riparian vegetation. E_s is the irradiance at the water surface after shading from topography and riparian vegetation, where s is the shading coefficient. E_0 is the irradiance that enters the water column after reflection at the air-water interface, where r is the reflection coefficient. E_{bed} is the irradiance at the riverbed after attenuation from the water column, which is dictated by the optical water quality (via the diffuse attenuation coefficient, K_d) and water depth (y).

ture including its type, height, density, and spatial distribution [*Song and Band*, 2004]. Channel geometry refers to the three spatial dimensions of planform, width, and depth. Planform and width augment or mitigate terrestrial shading by influencing the size of the canopy opening relative to the sunpath.

[5] Once light enters the water column, the amount reaching the riverbed (i.e., benthic light) is influenced by water depth, optical water quality and hydrologic regime. Optical water quality is the biogeochemical property that dictates the rate of light attenuation with depth and is set by the relative proportions of pure water, chromophoric dissolved organic matter, suspended sediment, particulate organic matter, and phytoplankton [*Kirk*, 1994]. Optical water quality can vary widely spatially along a river [*Davies-Colley*, 1987; *Julian et al.*, 2008] and temporally with discharge [*Smith et al.*, 1997; *Julian et al.*, 2008]. Hydrologic regime (the frequency, magnitude, timing, duration, and variability of streamflow [*Poff et al.*, 1997]) directly influences optical water quality and water depth, which in turn dictate the irradiance at depth in a river [*Smith et al.*, 1997; *Julian et al.*, 2008].

[6] Most previous riverine light studies have only assessed the control of optical water quality [*Davies-Colley*, 1987; *Davies-Colley and Close*, 1990; *Davies-Colley et al.*, 1992; *Koch et al.*, 2004; *Phlips et al.*, 2000]. The aquatic controls of optical water quality and hydrologic regime have been concomitantly addressed by only a few studies [*Davies-Colley*, 1990; *Smith et al.*, 1997]. The terrestrial controls of topography, riparian vegetation, and channel geometry have been concomitantly addressed by only a few studies as well [*Davies-Colley and Payne*, 1998; *Davies-Colley and Quinn*, 1998]. The most comprehensive riverine light studies have assessed topography, riparian vegetation, channel geometry, and optical water quality [*DeNicola et al.*, 1992; *Taylor et al.*, 2004], with hydrologic regime omitted. Further, all of the above studies have been site-specific. A comprehensive, explicit, and adaptable framework for characterizing light regimes in rivers has yet to be developed.

[7] The goal of this study was to develop a comprehensive and empirically based benthic light availability model (BLAM). Specific objectives were to quantify the amount of light attenuation by each hydrogeomorphic control, derive a comprehensive expression that incorporates both the spatial and temporal variability of these controls, and apply this model to rivers with a wide range of physical characteristics. First, we outline the analytical framework of BLAM for predicting photosynthetically active radiation (PAR: 400–700 nm) at the riverbed. Second, we apply BLAM to two dissimilar systems: a large, turbid river, and a small, optically clear river. Third, we compare model results of these two rivers to assess the dominant controls on both temporal and spatial light availability for rivers in general. Fourth, we assess the accuracy of BLAM by comparing modeled and measured PAR values at a transect in one of our study reaches. Finally, we provide examples of applications

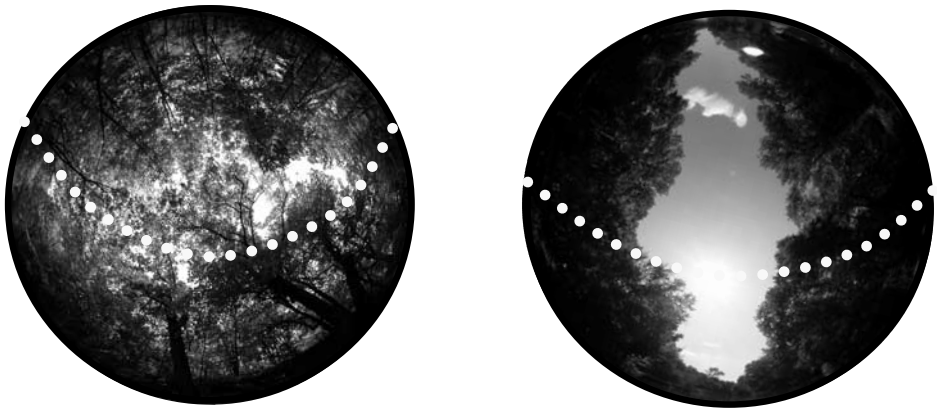

Figure 2. Hemispherical canopy photos of transects at (A) Big Spring Creek (BSC) and (B) Deep River (DR). The orientation of the BSC transect is West-East (azimuth = 90°) and the orientation of the DR transect is South-North (azimuth = 0°). Both transects are forested. The DR transect has an open canopy because of its greater width, 34 m compared to 6 m for the BSC transect. The dotted white line represents the sunpath on 27 June for BSC and 27 August for DR.

for BLAM and how readily available or commonly collected data can be used to assess light regimes at other sites.

2. Methods

2.1. Model Development

[8] To quantify benthic light availability, we combined previously developed and verified optical and hydrological methods. The first-order control on light availability is above-canopy PAR (E_{can}) in mol m^{-2} d^{-1}, where one mol equals 6.02×10^{23} photons. E_{can} is the total PAR (as irradiance) available to the river before any shading from topography or riparian vegetation (Figure 1). E_{can} can be obtained directly from a local weather station, measured directly with a PAR sensor, or modeled using solar simulation software.

[9] Topography and riparian shading decrease the intensity of PAR at the water surface, reducing E_{can} to E_s (Figure 1). We refer to the ratio of E_s:E_{can} as the shading coefficient (s), where s decreases with increased shading. The shading coefficient can be derived from numerous methods [see *Davies-Colley and Payne*, 1998; *Davies-Colley and Rutherford*, 2005], but we prefer the "canopy photo method," where a hemispherical canopy photograph is overlaid by the sunpath to calculate how much solar radiation is transmitted through openings in the canopy (Figure 2). After review of all the methods to quantify stream shade and several pilot studies, we found that this method provided the best combination of precision, simplicity, time-efficiency, versatility, and affordability. Most other methods used to quantify stream shade (e.g., clinometer, densiometer, and solar pathfinder) assume an opaque canopy, which can underestimate transmitted PAR by as much as 85% [*Chazdon and Pearcy*, 1991]. The canopy photo method was designed for forestry applications [*Evans and Coombe*, 1959], but has been successfully used to quantify stream shade [*Taylor et al.*, 2004].

[10] Reflection at the air-water interface decreases the intensity of PAR that enters the water column, reducing E_s to E_0 (Figure 1). We refer to the ratio of E_0:E_s as the reflection coefficient (r). The value of r can be found in situ by measuring PAR immediately above (E_s) and below (E_0) the water surface. Alternatively, r can be estimated using Fresnel's formula [*Kirk*, 1994; *Mobley*, 1994]. The product of E_{can}, s, and r is the total PAR that enters the water column.

[11] Once light enters the water column, it is attenuated exponentially with depth due to scattering and absorption by dissolved and particulate constituents. The PAR at depth in the river is thus derived using a simple exponential model [*Kirk*, 1994]:

$$E_d(y) = E_0 \cdot e^{-K_d \cdot y} \tag{1}$$

where $E_d(y)$ is downward PAR in μmol m^{-2} s^{-1} at depth y in m, and K_d is the diffuse attenuation coefficient for downward PAR in m^{-1}. K_d is predominantly set by the optical water quality, and to a lesser degree by the solar zenith angle and the ratio of diffuse to direct light. K_d can be normalized to remove the effects of solar zenith angle and ratio of diffuse to direct light [see *Gordon*, 1989], but for most waters dependence of K_d on these two variables is minimal [*Baker and Smith*, 1979; *Zheng et al.*, 2002].

[12] Combining equation (1) with the quantifications of shading and reflection allows calculation of PAR at the streambed (E_{bed}) in mol m^{-2} d^{-1} at one location in time:

$$E_{bed} = (E_{can} \cdot s \cdot r)e^{-K_d \cdot y} \tag{2}$$

Spatial variability of E_{bed} (i.e., longitudinally along the river) can be derived by adjusting the shading and depth (s and y). The other parameters of E_{can}, r, and K_d do not vary appreciably along a river reach, defined here as a length of river with no major confluences and longitudinally consistent optical water quality.

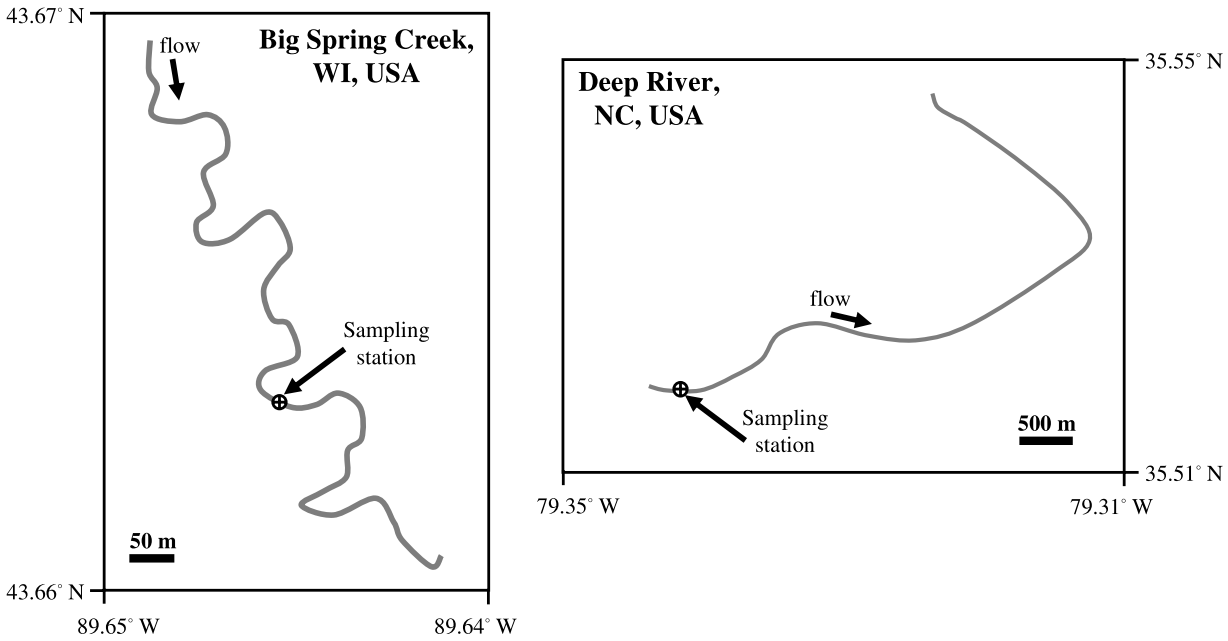

Figure 3. Big Spring Creek and Deep River study reaches. Sampling stations are where discharge was measured and temporal benthic light availability was assessed.

[13] In addition to spatial distributions, temporal variability of E_{bed} (i.e., at-a-station over time) can be quantified. We do this by relating y and K_d to water discharge (Q):

$$y = \alpha Q^{\nu} \tag{3}$$

$$K_d = \beta Q^{\omega} \tag{4}$$

where α, β, υ, and ω are rating parameters for y and K_d. We used the power function to relate both variables to Q based on previously developed empirical evidence from *Leopold and Maddock* [1953] for water depth and *Davies-Colley* [1990] for optical water quality. The combination of these two relations modifies equation (2) into a temporally variable form:

$$E_{bed} = (E_{can} \cdot s \cdot r)e^{-\alpha\beta Q^{(\nu+\omega)}}. \tag{5}$$

Equation (5) therefore predicts the temporal variations in benthic light availability as a function of discharge variability, while equation (2) predicts spatial variations in benthic light availability through a river reach. We focus here on light availability at the channel bed (E_{bed}) because it provides a relatively fixed datum, is the minimum value of underwater irradiance, and is the relevant quantity for benthic plant growth. This approach, however, can be used to predict light availability at any depth in the water column by simply adjusting y in equation (2).

2.2. Study Sites

[14] We applied BLAM to two river reaches: Big Spring Creek (BSC), a small, relatively clear river whose hydrology is driven by groundwater; and Deep River (DR), a large, relatively turbid river whose hydrology is predominantly influenced by surface runoff. The dissimilarities between these two systems allowed us to (1) investigate light regimes over a large range of physical characteristics and (2) display quantitative outputs for a river influenced more by terrestrial controls (BSC) versus one influenced more by aquatic controls (DR).

[15] Big Spring Creek is a 2nd-order spring-fed river located in the Central Plain of Wisconsin near Big Spring, WI (Figure 3). The BSC study reach was a 1.3 km section downstream of Big Spring Dam, a small run-of-river dam. Being a run-of-river dam, it did not alter the hydrology of BSC and comparisons between upstream (of the dam) and downstream stations revealed that downstream optical water quality was not significantly affected by the dam [*Julian et al.*, 2008]. There were no major tributaries and optical water quality was longitudinally consistent along the entire study reach (J. P. Julian, unpublished data, 2006). Land cover in its 21.1-km^2 watershed was mostly agriculture (46%), followed by forest (31%), grassland (21%), and wetland (2%). The discontinuous riparian corridor of BSC was composed of a mixture of reed canary grass (*Phalaris arundinacea*) and mixed-hardwood forest.

[16] Deep River is a 6th-order river located in the Central Piedmont of North Carolina near Carbonton, NC (Figure 3). The DR study reach was the 5.8 km section downstream of the former Carbonton Dam, which was removed in December 2005. There were no major tributaries and optical water quality was longitudinally consistent along the entire study reach (J. P. Julian, unpublished data, 2006). The 2770-km^2 watershed was dominated by forest (72%), followed by agriculture (25%), and urban (3%) land cover. Most of the urbanization in the basin was located in the headwaters, which together with its heavily entrenched channels, lead to high, flashy flood flows during storms. The nearly continuous riparian corridor of DR was composed of mixed-hardwood forest.

2.3. Data Collection and Model Inputs

2.3.1. Above-Canopy PAR (E_{can})

[17] We modeled E_{can} with Gap Light Analyzer (GLA) software [*Frazer et al.*, 1999], using the parameters in

Appendix A and the respective locations and elevations of BSC and DR. From GLA, we derived an average daily E_{can} for BSC during 15 May to 15 September and an average daily E_{can} for DR during 1 May to 30 September. We also obtained actual daily E_{can} values from the UV-B Monitoring and Research Program [*U.S. Department of Agriculture (USDA)*, 2007], which reported 3-min averages of 20-s readings from a *LI-COR* quantum sensor. Sites NC02 (60 km NE of DR) and WI02 (115 km N of BSC) were used for DR and BSC, respectively.

2.3.2. Reflection Coefficient (r) and Diffuse Attenuation Coefficient (K_d)

[18] We measured r and K_d at various locations and discharges along the study reaches using a *LI-COR* LI-192 underwater quantum irradiance (PAR) sensor. All measurements were taken at unshaded locations during full sun conditions between 15 May to 15 September 2006, between 0900–1500 local standard time, and using 15-s averages. We calculated r (E_0/E_s) by taking PAR measurements directly above the water surface (E_s) and at 1 cm below the water surface which we extrapolated to zero depth (equation (1)) to obtain E_0. A total of 27 and 25 r measurements were taken at BSC and DR, respectively. In addition to E_0, we measured PAR at the riverbed (E_{bed}) and at 10-cm intervals between these two depths. We derived K_d from the linear regression coefficient of ln $E_d(y)$ with respect to y (equation (1)). A total of 34 and 21 K_d measurements were taken at BSC and DR, respectively.

2.3.3. Shading Coefficient (s) and Water Depth (y)

[19] We used synoptic sampling to quantify the within-reach variability of s and y. We used a *Nikon Coolpix 4500* camera with fisheye lens to collect digital hemispherical canopy photos along the study reaches, which we processed and analyzed with GLA according to *Frazer et al.* [1999] to obtain E_s and s. We took 39 canopy photos along the channel centerline of BSC on 27 June 2006, with an average distance of 33 m between photos. We took 22 canopy photos along the channel centerline of DR on 27 August 2006, with an average distance of 264 m between photos. Photo locations were selected based on changes in channel width, canopy structure, and channel orientation (azimuth).

[20] We quantified y along the channel centerline of both study reaches using longitudinal profiles surveyed with a total station (*Trimble* 3350DR) and graded prism rod at baseflow conditions. We measured 129 locations along BSC on 15 June 2005 with an average interval of 10 m, and 67 DR locations on 12 September 2005 with an average interval of 86 m. Survey locations were selected based on changes in channel slope and water depth.

2.3.4. Temporal Sampling

[21] At each river, we established a fixed sampling station where we quantified depth, discharge, and turbidity. Temporal trends in these variables were assessed at a station 0.75 km downstream of the dam on BSC and 0.25 km downstream of the former dam on DR (Figure 3). Water depth was measured every 15 min by stage recorders (*Intech WT-HR 2000* for BSC and *HOBO 9-m* for DR). We calculated discharge (Q) using stage-Q rating curves developed with in-situ Q measurements taken with a *Marsh-McBirney* current meter. We estimated flood discharges at DR with the weighted area method [*Gordon et al.*, 2004], using a downstream USGS gage (#02102000) for a reference Q. All reported Q and y are daily average values.

[22] The rating parameters α and υ were derived from the regression of y versus Q (equation (3)), and β and ω were derived from the regression of K_d versus Q (equation (4)). We used turbidity (T_n) as an intermediate regressor (i.e., K_d was first regressed with respect to T_n, then T_n was regressed with respect to Q) due to the impracticality of measuring K_d during high flows. Because of the dominance of particulates on light attenuation in rivers, riverine optical water quality can be characterized fairly accurately using T_n measured in nephelometric turbidity units (NTU) with a turbidimeter [*Kirk*, 1994; *Julian et al.*, 2008; *Davies-Colley and Nagels*, 2008]. We measured T_n with a *HACH 2100P* turbidimeter from water samples collected during various flow periods (Appendix B).

2.4. Data Analysis

2.4.1. Statistical Methods

[23] To assess the dominant controls on benthic light availability, we compared correlations between E_{bed} and the parameters of BLAM (equations (2) and (5)). One-way analysis of variance (ANOVA; $p < 0.05$) was used to test for differences in s among various riparian communities and channel orientations. We classified riparian community as forest, grass, or mixed, and channel orientation by the four azimuthal axes: 0–180°, 45–225°, 90–270°, and 135–315°. We used JMP IN 5.1 (*SAS Institute*, Cary, NC) to perform all statistical tests.

[24] We also used JMP IN 5.1 to perform Monte Carlo simulations that quantified the frequency of daily E_{bed} for an independent randomly selected E_{can} and an independent randomly selected Q, which are the two temporally variable parameters in equation (5). We used 10,000 iterations (paired random samples) for each site, selecting from measured values of E_{can} (via the weather station) and Q (via the stage recorder). Distributions were tested for normality using the Kolmogorov-Smirnov test statistic (D), where $D < 0.05$ indicated a normal distribution.

2.4.2. Effect of Channel Orientation on the Shading Coefficient

[25] While the effects of channel width and canopy structure on s are intuitive (i.e., increased width increases s, increased canopy area and density decreases s), the effect of channel orientation on s is more complicated and has rarely been considered in light availability studies. We quantified the variation in s as a function of channel orientation by keeping width and canopy structure constant, which we accomplished by rotating the canopy photos in 45° increments and reanalyzing in GLA (eight analyses for each photo). For example, by rotating the canopy photo 90° in Figure 2B, we changed its orientation from South-North to West-East without altering its width or canopy structure. This technique was performed for four scenarios: closed canopy (forested banks, narrow channel), open canopy (forested banks, wide channel), half canopy (one grassed bank, one forested bank), and no canopy (grassed banks).

2.4.3. Model Accuracy Assessment

[26] In order to assess the accuracy of BLAM, we compared modeled daily E_{bed} (equation (5)) to actual daily E_{bed} (via PAR sensor). We measured E_{can}, E_s, E_0, and E_{bed}

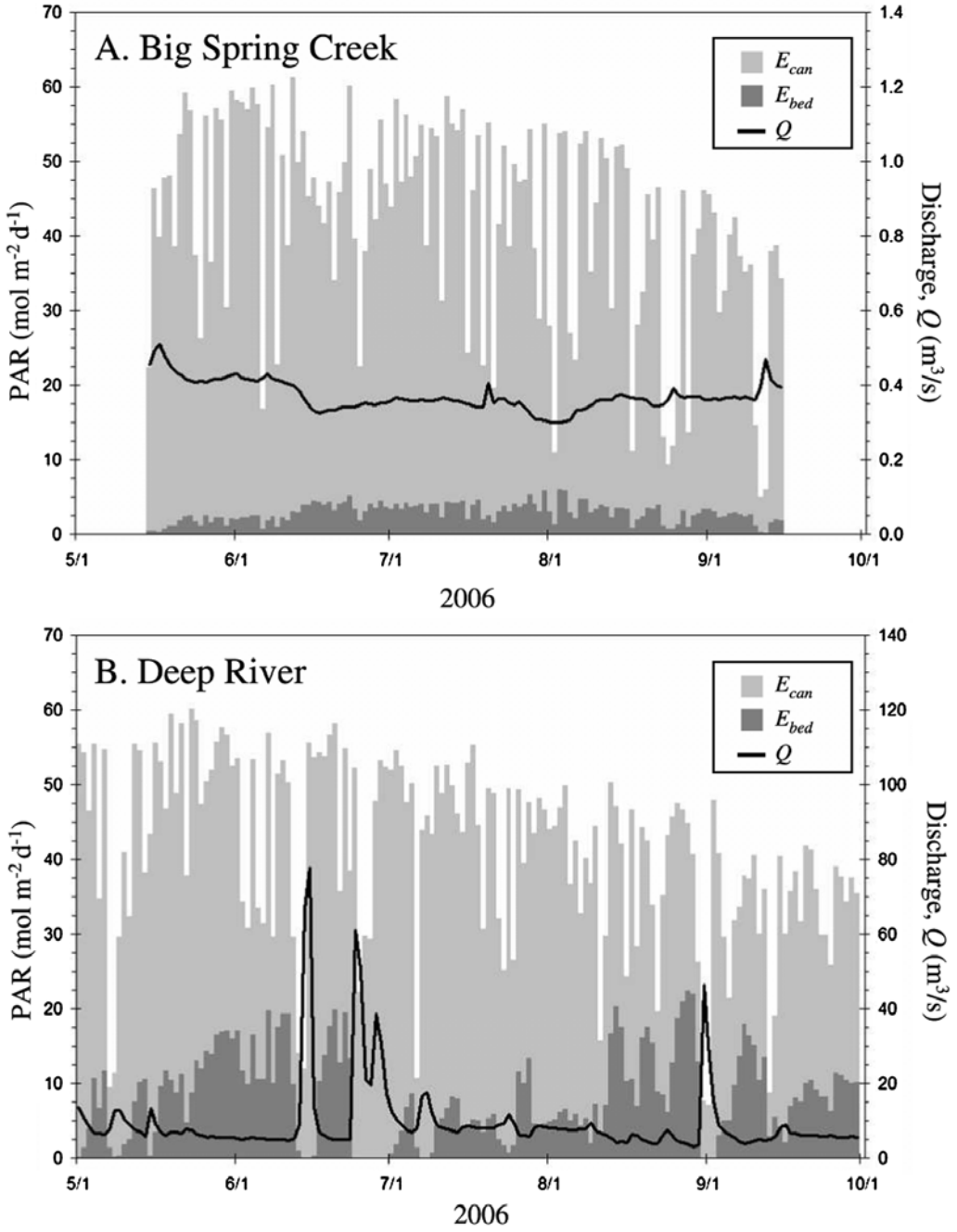

Figure 4. Temporal distribution of daily above-canopy PAR (E_{can}), discharge (Q), and benthic PAR (E_{bed}) at (A) Big Spring Creek and (B) Deep River. Note the different secondary y axes for Q between the study sites.

continuously at BSC with four PAR sensors during 16–25 June 2006. E_{can} was monitored in 1-min intervals with a PAR sensor (HOBO, *Onset*) placed in a nearby open field. The other three PAR sensors (LI-192, *LI-COR*) were set in an array in BSC at a transect 175 m downstream of the sampling station. We attached these three sensors to a metal rod driven into the bed of the channel, with one sensor located just above the water surface, one immediately below the water surface, and one on the riverbed to measure E_s, E_0, and E_{bed}, respectively. The three sensors were connected to a *LI-COR* LI-1400 data logger, which recorded PAR in 15-min intervals. These measurements were integrated and summed to obtain daily PAR. We leveled all four sensors with a bubble level and placed a mesh barrier upstream of the in-channel array to prevent debris from collecting around the sensors. The E_{bed} sensor was disturbed on 21 June, leaving 9 daily E_{bed} values. The E_0 sensor malfunctioned 18–22 June, leaving only 5 daily E_0 values. We also monitored daily E_s with PAR sensors (HOBO, *Onset*) placed at two other transects in BSC: one located at the sampling station (14–23 June 2006) and the other 520 m upstream of the sampling station (25–26 June 2006).

Table 1. BLAM Input Parameters for Big Spring Creek (BSC) and Deep River (DR)[a]

	Temporal		Spatial	
Parameter	BSC	DR	BSC	DR
E_{can}, mol m^{-2} d^{-1}	(5.04–61.23)	(7.10–60.21)	39.83	39.68
s	0.17	0.78	(0.15 to 0.94)	(0.52 to 0.81)
r	0.92	0.93	0.92	0.93
y, m	αQ^{υ}	αQ^{υ}	(0.23–1.26)	(0.34–3.55)
α	1.64	0.15	na	na
υ	0.49	0.67	na	na
K_d, m^{-1}	βQ^{ω}	βQ^{ω}	0.60	1.84
β	32.40	0.18	na	na
ω	3.69	1.31	na	na
Q	(0.30–0.51)	(3.17–77.79)	na	na

[a]Temporal parameters apply to the sampling station only. Spatial parameters apply to baseflow only. Parentheses indicate the parameter is variable, inside of which is the range of values for the study period. Parameters that are not applicable to the calculation of E_{bed} are labeled "na."

2.5. Model Assumptions and Limitations

[27] BLAM (i.e., equations (2) and (5)) is a one-dimensional model that assumes the river is well-mixed with no lateral variation in optical water quality. This assumption is not valid for river sections with large dead-water zones and sections directly below confluences [*Kenworthy and Rhoads*, 1995]. BLAM also does not take into account shading by aquatic biota, such as aquatic macrophytes. While we only assessed daily benthic PAR in the center of the channel, our approach can be used to assess light availability at any wavelength, depth, lateral distance, and time step.

[28] We performed all of our measurements and analyses when Leaf Area Index (LAI) was greater than 90% of annual maximum. This period of >90% LAI was conservatively estimated from previous studies on seasonal leaf dynamics in the study site's region: central North Carolina (1 May to 30 September [*Palmroth et al.*, 2005]) and central Wisconsin (15 May to 15 September [E. H. Stanley, unpublished data, 2005]). By confining our model results to these periods of >90% LAI, we effectively removed seasonal variations in E_{can} and E_s, and minimized seasonal variations in r and K_d. BLAM can be used to investigate seasonal variability in E_{bed} with additional measurements, but this analysis was beyond the scope of the present study.

3. Results

3.1. Controlling Parameters

3.1.1. Hydrology and Channel Geometry

[29] BSC had a baseflow water surface width of 7.5 ± 1.8 m (mean ± standard deviation) and depth of 0.6 ± 0.2 m over the 1.3-km study reach. Its flow was relatively constant (Figure 4A and Table 1). Average Q was 0.37 ± 0.04 m^3/s and only 4 stormflows with peaks greater than 0.40 m^3/s (75th percentile) occurred during the study period. Water depth at the BSC sampling station ranged 0.9–1.2 m and averaged 1.0 ± 0.1 m. Spatially, y was variable along the sand-bed channel of BSC, fluctuating between 0.2 and 1.3 m during baseflow. Channel orientation in BSC changed often as a result of its high sinuosity (Figure 3).

[30] DR had a much larger channel with a baseflow water surface width of 35.0 ± 4.7 m and depth of 1.2 ± 0.6 m. Discharge at DR was greater and considerably more variable

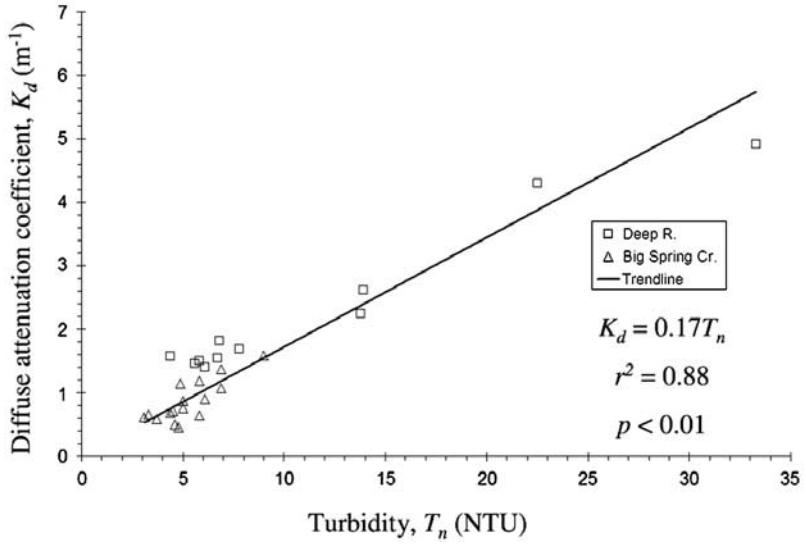

Figure 5. Diffuse attenuation coefficient (K_d) versus turbidity (T_n) for Big Spring Creek and Deep River.

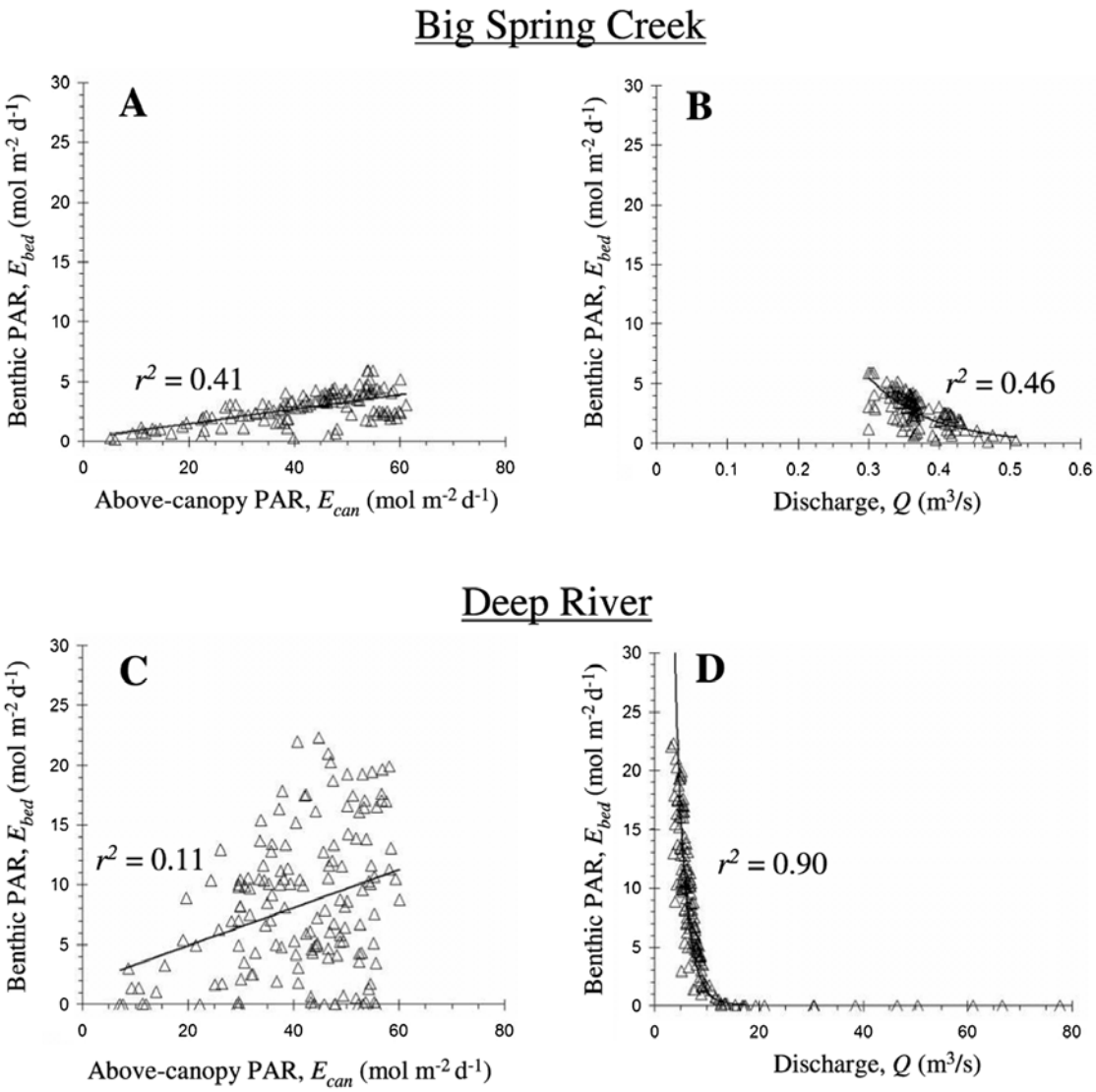

Figure 6. Temporal comparisons of benthic PAR (E_{bed}) with above-canopy PAR (E_{can}; A, C) and discharge (Q; B, D) for Big Spring Creek and Deep River, respectively. On the basis of equation (5), linear regression was used for Figures 6A and 6C, and exponential regression was used for Figures 6B and 6D.

(Figure 4B and Table 1), as average Q was 9.6 ± 10.7 m^3/s. During the study period, DR experienced 11 stormflows with peaks greater than 8.6 m^3/s (75th percentile). At the DR sampling station, y ranged 0.3–2.9 m and averaged 0.6 ± 0.4 m. Spatially, y was highly variable along the gravel bed channel of DR, ranging 0.3–3.6 m during baseflow. The low sinuosity of DR resulted in relatively few changes in channel orientation (Figure 3).

3.1.2. Terrestrial Shading

[31] Daily above-canopy PAR (E_{can}) at both sites fluctuated considerably in response to varying degrees of cloudiness (Figure 4 and Table 1). Between 15 May and 15 September 2006, E_{can} at BSC averaged 42.0 ± 13.9 mol m^{-2} d^{-1}, which agreed closely with the GLA prediction of 39.8 mol m^{-2} d^{-1}. Between 1 May and 30 September 2006, E_{can} at DR averaged 41.2 ± 12.4 mol m^{-2} d^{-1}, which also agreed closely with the GLA prediction of 39.7 mol m^{-2} d^{-1}.

[32] The proportion of E_{can} remaining after terrestrial shading varied widely along the BSC study reach due to changes in the riparian community (Table 1). Spatially averaged s was 0.51 ± 0.25, i.e., approximately 51% of the available daily PAR passed through the canopy and reached the water surface over the entire reach. s was more consistent along DR due to a continuous and relatively uniform riparian corridor (Table 1) and averaged 0.68 ± 0.08. The fixed sampling stations at BSC and DR had an s of 0.17 and 0.78, respectively.

3.1.3. Aquatic Light Attenuation

[33] The proportion of E_s remaining after reflection at the air-water interface (r) was relatively constant at both sites, averaging 0.92 ± 0.03 at BSC and 0.93 ± 0.03 at DR. The water at BSC was much clearer than DR, where baseflow K_d was 0.60 ± 0.09 m^{-1} and 1.84 ± 0.39 m^{-1} for BSC and DR, respectively. The relationship between K_d and T_n for both rivers was: $K_d = 0.17T_n$ (r^2 = 0.88; Figure 5). The

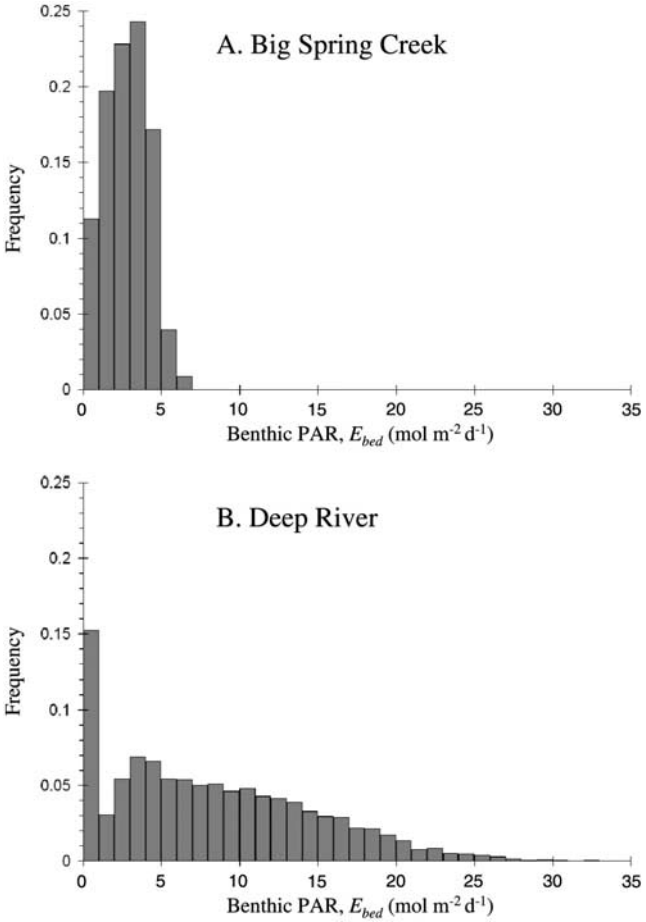

Figure 7. Magnitude-frequency distributions of benthic light availability (E_{bed}) at (A) Big Spring Creek and (B) Deep River. Histograms were constructed from Monte Carlo simulations using 10,000 iterations for each site.

relationship between T_n and Q was: $T_n = 190.57Q^{3.69}$ (r^2 = 0.54) for BSC, and $T_n = 1.04Q^{1.31}$ (r^2 = 0.85) for DR. Together these relationships produced the rating parameters between K_d and Q (equation (4) and Table 1).

3.2. Temporal Light Availability

3.2.1. Temporal BLAM Output

[34] Modeled benthic PAR (E_{bed}) at the BSC sampling station varied between 0.1 and 5.9 mol m^{-2} d^{-1} during 15 May to 15 September 2006 (Figure 4A) and average E_{bed} during this period was 2.8 ± 1.3 mol m^{-2} d^{-1}. Generally, E_{bed} at BSC was highest when E_{can} was high and Q was low (Figures 4A, 6A, and 6B). Benthic PAR at the DR sampling station varied from 0.0 to 22.3 mol m^{-2} d^{-1} during 1 May to 30 September, 2006 (Figure 4B). The average E_{bed} during this period was 8.2 ± 6.0 mol m^{-2} d^{-1} and E_{bed} was typically highest when Q was low (Figures 4B and 6D). Although the correlation was statistically significant, E_{can} could account for only 11% of the observed variation in E_{bed} at DR (Figure 6C).

3.2.2. Magnitude-Frequency Distribution of Benthic Light Availability

[35] The two temporally variable parameters in BLAM, assuming only summer conditions, are E_{can} and Q (Table 1). There was no dependence of Q on E_{can} (i.e., no multicollinearity) for BSC (p = 0.57) or DR (p = 0.15), which validated the use of Monte Carlo simulations at both sites. From these simulations and using equation (5), the possible range of E_{bed} was 0–7 mol m^{-2} d^{-1} for BSC and 0–33 mol m^{-2} d^{-1} for DR (Figure 7). E_{bed} for BSC was approximately normally distributed (D = 0.04) with a peak at 3–4 mol m^{-2} d^{-1} (Figure 7A). In contrast, E_{bed} for DR was nonnormally (D = 0.10), broadly distributed with two modes, one at 0–1 and the other at 3–4 mol m^{-2} d^{-1} (Figure 7B). Most importantly, for DR there were many E_{bed} values with similar frequencies, whereas for BSC, frequencies were dissimilar for the relatively few E_{bed} values.

3.3. Spatial Light Availability

3.3.1. Spatial BLAM Output

[36] Benthic PAR along the 1.3-km reach of BSC varied between 3.2 and 25.1 mol m^{-2} d^{-1} during baseflow (Figure 8A) with a reach average of 12.7 ± 6.7 mol m^{-2} d^{-1}. Generally, E_{bed} was highest in unshaded sections where s was high (Figure 9A). There was not a strong correlation between E_{bed} and y along BSC (Figure 9B). However, when divided into riparian groups, correlations between E_{bed} and y at BSC were stronger, with r^2 values of 0.25, 0.79, and 0.65 for forest, mixed, and grass, respectively.

[37] Benthic PAR along the 5.8-km DR study reach varied between 0.0 and 14.7 mol m^{-2} d^{-1} during baseflow (Figure 8B) with a mean of 4.4 ± 3.3 mol m^{-2} d^{-1}. High E_{bed} values usually occurred in shallow sections where y was low (Figure 9D). The correlation between E_{bed} and s at DR was relatively weak (Figure 9C). In sum, E_{bed} along BSC was well-predicted by shading but not depth, whereas E_{bed} at DR was well-predicted by depth but not shading.

3.3.2. Channel Geometry and Canopy Structure

[38] The two spatially variable parameters in BLAM are s and y (Table 1), both of which are influenced by channel geometry. Channel depth dictates y, while channel width and orientation, along with canopy structure, dictate s. Canopy structure was the major influence on s for BSC because of its wide variation in riparian community: forest (s = 0.26 ± 0.10, n = 15), grass (s = 0.80 ± 0.07, n = 13), and mixed (0.52 ± 0.07, n = 11). These three groups were significantly different with respect to s ($p < 0.01$). Width could only explain 21% of the variation in s along the entire BSC reach, and explained even less variation within riparian groups (r^2 = 0.01, 0.03, and 0.02 for forest, grass, and mixed, respectively). The difference in s among the four axes of channel orientation was only marginally significant (p = 0.06).

[39] Although y was the dominant control on E_{bed} along DR, s also affected E_{bed} because of its control on E_0. Compared to BSC, DR had a relatively uniform forested riparian corridor. The correlation between s and channel width was very weak (r^2 = 0.03) at DR, and there was no significant difference in s among the four axes of orientation (p = 0.79), which suggests that variation in s here probably resulted from the sum of independent variations in all three factors.

[40] The effect of channel orientation on s varied for different canopy structures. For a transect at BSC with a closed canopy, channel orientation did not change s by more than 0.06 (Figure 10). Similarly, for a transect at BSC with no canopy, channel orientation did not change s by more than 0.02. For a transect at BSC with a half canopy, channel

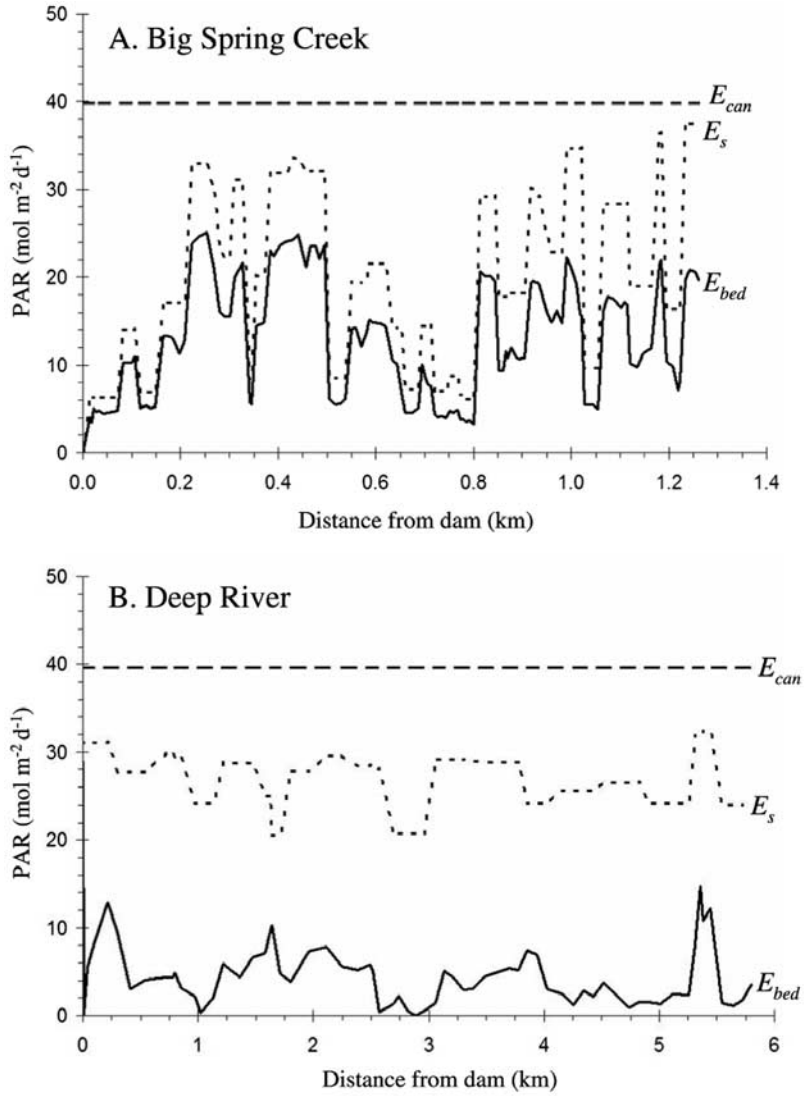

Figure 8. Longitudinal distribution of above-canopy PAR (E_{can}), below-canopy PAR (E_s), and benthic PAR (E_{bed}) during baseflow at (A) Big Spring Creek and (B) Deep River. Note the different x axes between the study sites.

orientation changed s by as much as 0.39. For a typical transect at DR with an open canopy, channel orientation changed s by as much as 0.20, with peaks at 90° and 270° (Figure 10). In all four canopy scenarios, the maximum s occurred at an azimuth of 90° (West-East). Thus given the same canopy structure and channel width, channel orientation has the potential to alter s considerably.

3.4. Comparisons Between Modeled and Actual Benthic PAR

[41] BLAM (equation (5)) consistently over-predicted E_{bed}, but did so within 39% on average for the period of 16–25 June 2006 (Figure 11 and Appendix C). BLAM predicted E_{bed} within 20% on four of the 9 d, and the greatest error was 92%. A considerable portion of the error resulted from the difference in s between the sensor and modeled values. GLA calculated an s of 0.67 at this site, while the sensors (E_s/E_{can}) measured an s of 0.56 ± 0.05. Substituting the actual s into equation (5) reduced the average error of BLAM to 15%. A PAR sensor placed at the BSC sampling station showed similar error in s, where GLA calculated 0.17 and the sensors measured 0.08 ± 0.01 (n = 7). However, a PAR sensor placed at another transect showed very little error in s, where GLA calculated 0.79 and the sensors measured 0.78 ± 0.01 (n = 2).

[42] Differences in K_d between sensor and modeled values also added model error. Using β and ω from Table 1, BLAM predicted a K_d of 0.58 ± 0.05 m^{-1} for the 9-d period, whereas the sensors ($\ln E_0 \ln E_{bed}^{-1} y^{-1}$) measured 0.85 ± 0.12 m^{-1}. Substituting the actual K_d and s from Appendix C into equation (5) reduced the average error of BLAM to 7% (Figure 11). There were relatively minor differences in the other parameters between modeled and measured values:

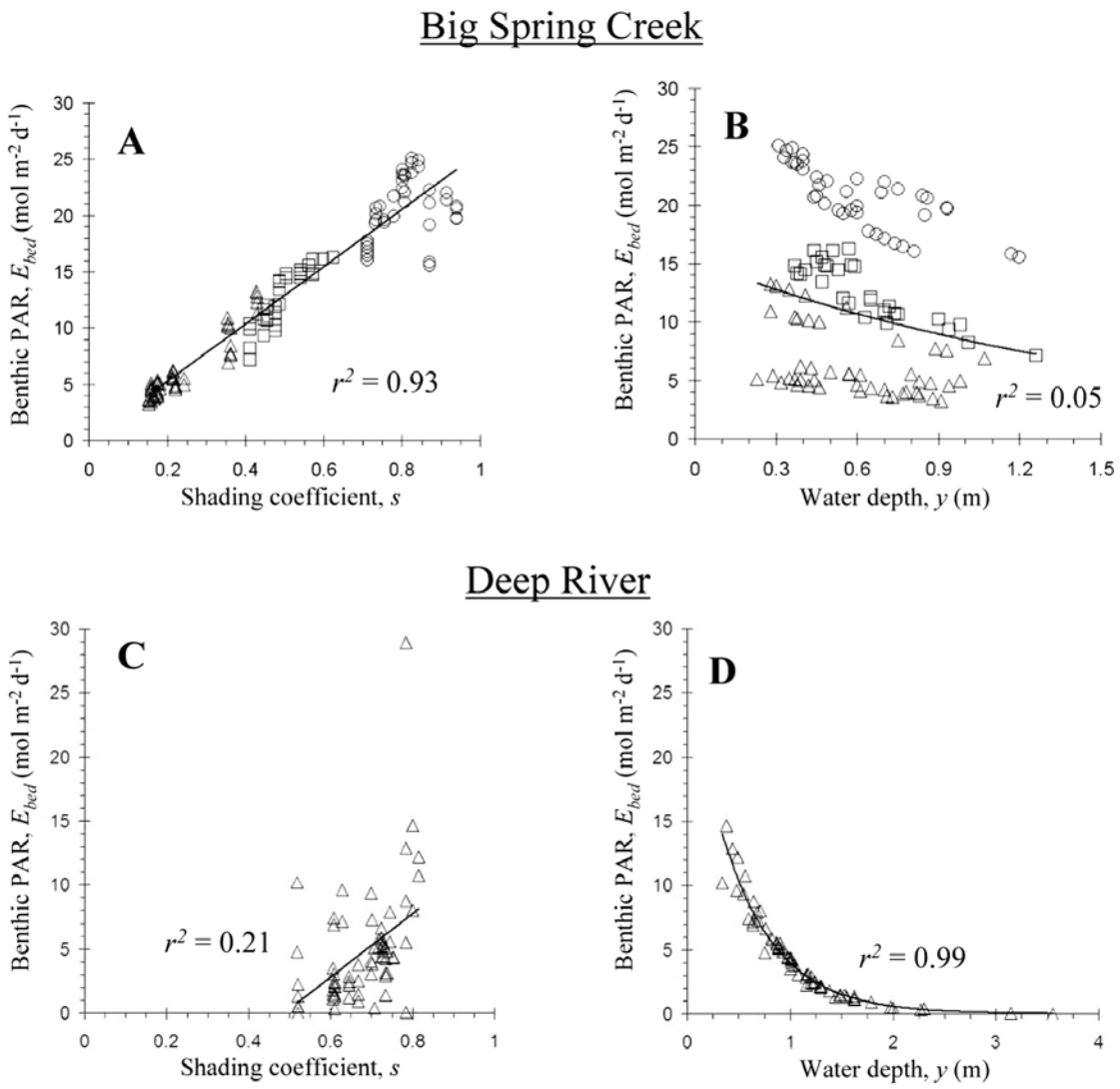

Figure 9. Spatial comparisons of longitudinal benthic PAR (E_{bed}) with shading coefficient (s; A, C) and water depth (y; B, D) for Big Spring Creek and Deep River, respectively. Triangles = forest, Squares = mixed, and Circles = grass. On the basis of equation (2), linear regression was used for Figures 9A and 9C, and exponential regression was used for Figures 9B and 9D.

E_{can} (BLAM: 43.0 ± 10.6 mol m^{-2} d^{-1}, Sensors: 40.7 ± 10.9 mol m^{-2} d^{-1}) and r (BLAM: 0.92 ± 0.03, Sensors: 0.88 ± 0.04).

4. Discussion

4.1. Controls on Riverine Benthic Light Availability

4.1.1. Atmosphere

[43] Atmospheric constituents are the first-order controls on light availability in rivers. Their enormous spatiotemporal variability and unpredictability [*Kirk*, 1994] prevented us from modeling E_{can} as a dependent variable. We therefore used E_{can} as the independent variable in BLAM. While solar simulation software (GLA) proved to be accurate within 5% of the average daily E_{can}, the weather station data were needed to derive actual frequencies of benthic light availability (Figure 7). The weather station data are also beneficial when correlations between ecological variables and E_{can} are sought [e.g., *Mulholland et al.*, 2001]. Daily E_{can} is likely to vary considerably in response to cloud cover (Figure 4) and therefore correlations of this nature require accurate measurements which can only be acquired from a local weather station or user-installed PAR sensor.

4.1.2. Terrestrial Controls

[44] Before solar irradiance enters the water column, its intensity is reduced by the terrestrial controls of topography, riparian vegetation, and channel geometry. Topography was not an effective control on light attenuation at either river due to their limited relief. Topography is however capable of being a dominant control on light availability in mountainous streams, canyon rivers, and heavily incised rivers [*Davies-Colley and Payne*, 1998; *Yard et al.*, 2005].

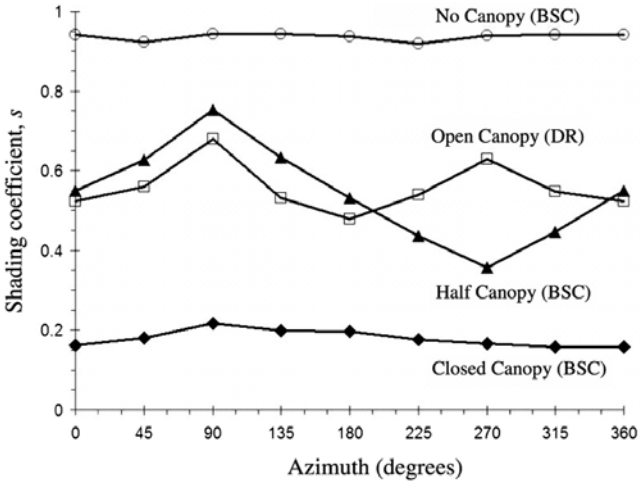

Figure 10. Effect of channel orientation (i.e., compass direction) on shading coefficients (s), which were derived from Gap Light Analyzer software and canopy photos from Big Spring Creek (BSC) and Deep River (DR). Canopy photos were rotated in 45° increments to obtain the entire range of channel orientations. "No Canopy" is a grassed transect at BSC (width = 7 m). "Open Canopy" is a forested transect at DR (width = 34 m). "Half Canopy" is a transect at BSC with the east bank grassed and the west bank forested (width = 8 m). "Closed Canopy" is a forested transect at BSC (width = 6 m).

[45] Riparian vegetation was a dominant control on E_{bed} at BSC because of its relatively narrow channel. In forested sections of BSC, riparian vegetation shaded as much as 85% of the incoming PAR. In contrast, riparian vegetation accounted for only a 32% reduction of E_{can} at the wider DR. This trend supports the common expectation that terrestrial shading decreases with increasing channel width [*Davies-Colley and Quinn*, 1998; *Vannote et al.*, 1980].

[46] Channel orientation can also mitigate or exaggerate the effect of terrestrial shading. The relative change in s caused by channel orientation was greatest at DR, which had an open canopy, and in sections of BSC with a half-canopy (Figure 10). In river sections with either a closed canopy or no canopy, the orientation of the channel does not significantly alter s because of the uniform distribution of canopy gaps relative to the sunpath. For river sections with an open canopy, riparian shading is the most exaggerated (lowest s) by North-South orientations because of the higher opacity of the channel margins and the smaller window for direct solar radiation transmission (see Figure 2B for context). Conversely, East-West orientations provide a larger window for direct solar radiation transmission and orient the sunpath over the upper canopy, which has more gaps than the lower canopy. Our finding that maximum s occurred at an azimuth of 90° for all riparian vegetation scenarios confirmed this relation. The relationship between channel orientation and topographic shading follows a similar trend as long as the sun angle is higher than the local topography; however, when the sun angle is lower than the local topography (e.g., deep canyons or during winter) an inverse relationship is more likely where maximum s occurs in North-South orientations [*Yard et al.*, 2005].

4.1.3. Aquatic Controls

[47] While the boundary conditions of rivers (terrestrial controls) create spatial variation in light availability within a season, the aquatic controls of hydrologic regime and optical water quality create temporal variation. In small, spring-fed rivers such as BSC, this temporal variation may not be large due to a relatively constant hydrologic regime and optical water quality. Further, temporal variation of E_{bed} in small rivers is likely to be suppressed by the influence of terrestrial shading. However, for most rivers, the variation in benthic light availability is likely to be quite large due to the variability in Q, which dictates the temporal variability in y [*Leopold and Maddock*, 1953] and K_d [*Davies-Colley*, 1990]. While the correlation between y and Q was strong, the correlation between K_d and Q was far more variable. This greater variation is largely the result of interstorm and seasonal effects on optical water quality [*Julian et al.*, 2008].

[48] The use of T_n as an intermediate regressor also added variation to the correlation. However, we found a strong and similar correlation between K_d and T_n at both study sites (Figure 5), and therefore suggest T_n as a predictor of K_d in nontidal freshwater rivers with low chromophoric dissolved organic matter (CDOM). Indeed, *Davies-Colley and Nagels* [2008] found that T_n explained 95% of the variation in K_d for a wide range of rivers across New Zealand. For rivers with highly colored water or very low turbidity, including the effect of CDOM on K_d would likely improve K_d estimates [*Davies-Colley and Nagels*, 2008]. Additionally, their study showed that the relation between K_d and T_n is more likely to follow a power law trend (exponent ~0.5) when a wider range of K_d values is considered. In all, temporal variation of benthic light availability within river

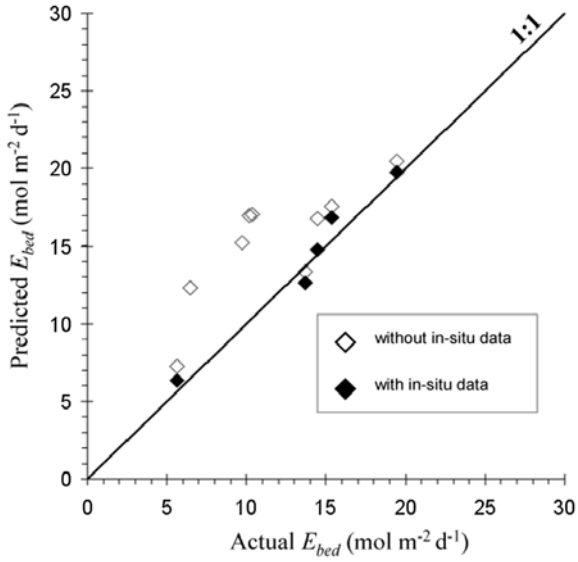

Figure 11. Predicted daily benthic PAR (E_{bed}) versus actual E_{bed} at BSC for 16–25 June 2006. Predicted E_{bed} was modeled using equation (5). Actual E_{bed} was measured with an underwater PAR sensor. In situ data include s and K_d derived from the sensor array (Appendix C).

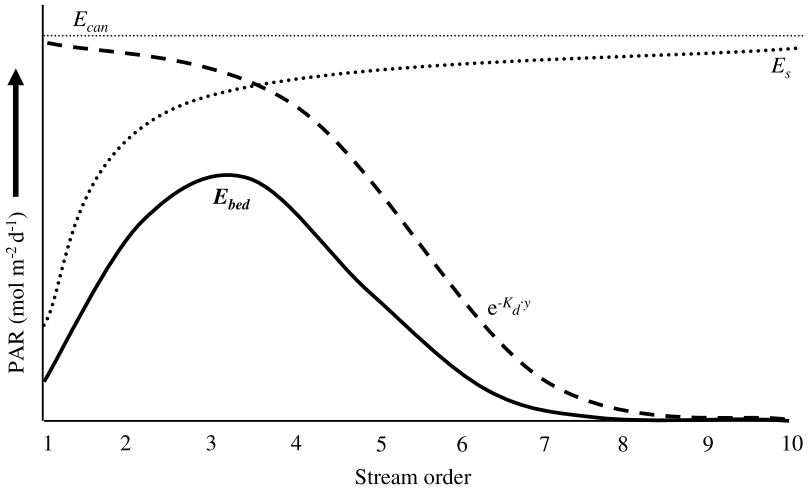

Figure 12. Benthic light availability along the river continuum of an idealized 10th-order river with a continuous forested riparian corridor. Benthic PAR (E_{bed}) was derived from equation (2), where E_{can} is above-canopy PAR, E_s is the intensity of PAR at the water surface after terrestrial shading, and $e^{-K_d y}$ is the inverse exponential product of depth (y) and the diffuse attenuation coefficient (K_d). The product of $e^{-K_d y}$ is a dimensionless proportion, with a value of $\sim$1 in the headwaters and a value of $\sim$0 at the outlet. The influence of aquatic attenuation thus increases in the downstream direction, whereas the influence of terrestrial shading decreases in the downstream direction.

reaches is likely to be substantially and predominantly driven by variability in river depth and optical water quality.

4.2. Small Versus Large Rivers

[49] Overall, DR had less spatial variability (Figure 8) but greater temporal variability (Figures 4 and 7) in E_{bed} than BSC. The magnitude-frequency distribution of benthic light availability in rivers is affected by all the parameters in equation (5), but it is mostly governed by the temporal distributions of E_{can} and Q. Because of the dominating influence of s on E_{bed} for small rivers such as BSC, their temporal variability in E_{bed} is likely to follow the trend of E_{can}. In basins with frontal weather patterns, this trend is characterized by an approximately normal distribution in which most days have an intermediate E_{can} and few days have very low or very high E_{can}. For large rivers such as DR, Q is likely to be the dominant influence on E_{bed}; however, E_{can} also affects the temporal distribution of E_{bed} because it is the first-order control on light availability. Therefore the magnitude-frequency distribution of benthic light in large rivers is likely to have a broad and more bimodal distribution in which one peak is set by E_{can} and the other by Q. For example, the left peak in Figure 7B was caused by the high frequency of floods in DR, which lead to elevated turbidity for long periods [*Julian et al.*, 2008]. This elevated turbidity attenuates most of the underwater light before it reaches the bed. The right peak in Figure 8B was caused by the distribution of E_{can}, which is similar to that of BSC. Overall, s sets the maximum potential E_{bed}, while Q sets the potential range and frequency of E_{bed}.

[50] Along the river continuum (from headwaters to mouth), the influence of shading on E_{bed} decreases due to the mitigating effect of width on s. Conversely, the effect of y and K_d on E_{bed} increases with increasing river size due to the increase in depth and turbidity in the downstream direction. Using equation (2) and assuming a continuous forested riparian corridor, the combined effect of terrestrial shading and aquatic attenuation produces a longitudinal distribution of E_{bed} where it is low in the headwaters, high in the middle reaches, and essentially zero in the higher-orders (Figure 12). In general, s is the dominant control on E_{bed} in small rivers and y is the dominant control on E_{bed} in large rivers (Figure 9). The influence of y on E_{bed} increases with increasing turbidity. These above relations were developed from reach-scale comparisons and expected longitudinal patterns. In order to verify the trends in Figure 12, basin-scale surveys of light availability are needed.

4.3. Applications of BLAM

4.3.1. Required Data and Accuracy

[51] BLAM incorporates the six major controls on light availability in rivers, and allows for both temporal and spatial variation in these controls. Using our approach, the minimum information needed to characterize light availability at one location in a river is a canopy photo and some measure of optical water quality (e.g., T_n). Applying our method to an entire reach would require measures of depth and additional canopy photos. Temporal characterization of light availability would require knowledge of the hydrologic regime and its relationship with y and K_d. For any application of BLAM, the extent of data collection would be determined by the desired precision.

[52] Overall, BLAM provided fairly accurate estimates of E_{bed} (Figure 11). Most of the model error was in s and K_d. We derived the model value of s from GLA using generalized and average configuration parameters. These parameters are highly variable in both space and time

[*Kirk*, 1994], and are the primary control on canopy light transmission [*Song and Band*, 2004]. To better characterize *s*, one would therefore need more spatiotemporally explicit values of the configuration parameters used in GLA.

[53] We derived the model value of K_d from measurements taken in unshaded locations during midday and full sun conditions. Variations in the ambient light field are expected to only minimally affect K_d in most rivers due to their high scattering to absorption ratios [*Zheng et al.*, 2002]; however in optically clear rivers such as BSC, increased zenith angles (early morning and late afternoon) and reduced direct irradiance (cloudy and shaded) are likely to decrease K_d [*Gordon*, 1989]. Our model value was therefore probably more characteristic of the minimum K_d than the daily average K_d. Obtaining a daily average K_d for varying levels of cloudiness and streamside shade would involve greater sampling and more sophisticated techniques [e.g., *Davies-Colley et al.*, 1984] than we used, especially for optically clear rivers.

4.3.2. River Ecosystem Dynamics

[54] BLAM can be used to characterize spatial and temporal trends in river light regimes, however its greater utility is as a tool to investigate river ecosystem dynamics. Light is a first-order control on both abiotic (via the hydrological cycle, temperature, and photochemical reactions) and biotic (via temperature, photosynthesis, and visual perception) processes in rivers [*Wetzel*, 2001]. Further, it is the only control that exhibits a strong correlation to gross primary production over a wide range of streams [*Mulholland et al.*, 2001]. Yet light budgets are rarely developed for river ecosystem studies. BLAM provides a fairly simple, inexpensive (time and money), and precise tool for creating these budgets.

[55] If we can quantify the amount of solar radiation entering a river, we have a first approximation of one of the major components of ecosystem energy, which can then be used to assess metabolism [see *Brown et al.*, 2004]. One of the major metabolic processes in rivers is photosynthesis (or primary production) by algae and submersed aquatic macrophytes. All aquatic plants have a compensation irradiance, which is the amount of PAR required for photosynthesis to exceed respiration [*Kirk*, 1994], and these compensation points can be determined relatively easily for naturally occurring assemblages of macrophytes or algae. Thus by knowing how much PAR reaches the benthos, we can approximate net photosynthesis. For example, assuming a compensation irradiance of 3 mol m^{-2} d^{-1} for a typical macrophyte population [*Kirk*, 1994, p. 278], benthic photosynthesis would occur 46% of the days during the summer at BSC and 77% of the days during the summer at DR (Figure 7). Relations such as these calculated with BLAM can be used to investigate spatiotemporal trends in riverine vegetation, primary productivity, and metabolism. Other potential applications of BLAM include riparian zone management [*Kiffney et al.*, 2004], nutrient budgets [*Doyle and Stanley*, 2006], environmental maintenance flows [*Baron et al.*, 2002], stream restoration [*Scarsbrook and Halliday*, 1999], biotic behavioral adaptations [*Kelly et al.*, 2003], and feedbacks between geomorphology and ecology [*Bott et al.*, 2006]. Although the above references establish the ecological importance of light in rivers, the role of light in each of these areas has largely been underappreciated and not fully demonstrated.

5. Conclusions

[56] Compared to other aquatic ecosystems, rivers arguably possess the greatest spatiotemporal variability and complexity. This complexity has up to now prevented the development of a general framework in which to assess light regimes in rivers. By combining previously verified optical and hydrological methods, we were able to generate the benthic light availability model (BLAM) which calculates the intensity of PAR at the riverbed. BLAM links river hydrogeomorphology and benthic light availability by incorporating the light attenuation of topography, riparian vegetation, channel geometry, optical water quality, and hydrologic regime.

[57] The accuracy of BLAM is largely dependent on the accuracy of the techniques used to obtain *s* and K_d. We recommend that future studies assess the validity of these techniques, especially for varying degrees of cloudiness and shading. Further, we encourage testing on a wide variety of rivers, thereby improving upon the accuracy and range of empirical coefficients used in BLAM.

[58] We used BLAM to demonstrate how the spatiotemporal variations in hydrogeomorphic controls dictate benthic light availability in a small, optically clear river versus a large, turbid river. In addition to assessing the dominant controls on riverine light regimes, BLAM is a tool that can be used to investigate the role of light in river ecosystem dynamics and establish light availability targets in water resource management. BLAM also provides a framework for future models that characterize spatiotemporal variations of ultraviolet radiation and water temperature in rivers. Our ultimate objective in developing BLAM is that it will be a catalyst for more investigations and applications of the vital role of light in rivers.

Appendix A

[59] Table A1.

Appendix B

[60] Table B1.

Appendix C

[61] Table C1.

Table A1. GLA User-Defined Parameters

Parameter	Value
Projection	polar
Orientation	horizontal
Time step	1 min
Azimuth regions	36
Zenith regions	9
Solar constant	1367 W/m^2
Cloudiness Index	0.50
Spectral fraction	0.45
Beam fraction	0.50
Sky-region brightness	UOC model
Clear-sky transmission coefficient	0.60

Table B1. Turbidity Sampling at Big Spring Creek (BSC) and Deep River (DR)

	21–30 May 2006	14–16 Jun 2006	11–17 Jul 2006	29 Aug to 11 Sep 2006	24–26 Apr 2006	15–24 Jun 2006	24 Jun 2005 to 18 Sep 2006
Location	DR	DR	DR	DR	BSC	BSC	BSC
Method[a]	automated	manual	automated	automated	automated	automated	manual
Flow	baseflow	flood	baseflow	flood	baseflow	baseflow	baseflow/flood
Sample interval, h	12	~24	6	6	4	6	discrete
Sample number	22	3	23	54	11	33	22/2

[a]Automated samples were collected with a *Teledyne-ISCO* 6712.

Table C1. Predicted Versus Actual Benthic PAR in Big Spring Creek, WI

Source	PAR Sensor	PAR Sensor	PAR Sensor	PAR Sensor	Stage Recorder	Weather Station	BLAM	
Date (M/D/Y)	E_{can} (mol/m^2/d)	E_s (mol/m^2/d)	E_0 (mol/m^2/d)	E_{bed} (mol/m^2/d)	Q (m^3/s)	E_{can} (mol/m^2/d)	E^*_{bed} (mol/m^2/d)	E^*_{bed}/E_{bed}
6/16/2006	43.32	25.43	22.47	15.37	0.33	47.74	17.57	1.14
6/17/2006	46.39	26.47	22.16	14.44	0.32	43.99	16.81	1.16
6/18/2006	40.04	21.21	na	9.7	0.33	41.63	15.24	1.57
6/19/2006	46.45	22.43	na	10.34	0.33	47.23	17.06	1.65
6/20/2006	30.57	14.49	na	6.44	0.33	33.99	12.33	1.92
6/22/2006	40.31	25.59	na	10.16	0.34	49.81	16.95	1.67
6/23/2006	59.31	35.41	30.51	19.45	0.34	60.18	20.49	1.05
6/24/2006	39.80	23.13	22.09	13.71	0.34	39.52	13.35	0.97
6/25/2006	20.19	11.92	10.30	5.65	0.35	22.45	7.24	1.28

Actual values were collected with PAR sensors at a transect 175 m downstream of the sampling station during 16–25 June 2006. Values for 21 June are not reported because the E_{bed} sensor was disturbed on that day. The shading coefficient (s) for this site as derived by GLA was 0.67. All other temporal parameters used in BLAM are listed in Table A1. Data not available due to equipment malfunction are labeled "na." E^*_{bed} is the predicted benthic PAR according to equation (5), and E_{bed} is the actual benthic PAR measured with a PAR sensor.

[62] **Acknowledgments.** The project was supported by the National Research Initiative of the USDA Cooperative State Research, Education, and Extension Service (CSREES grant 2004-35102-14793). Special thanks to Bill Ginsler and the town of Big Spring, WI for site access. Derek Anderson, Richelle Baroudi, Zack Feiner, Victoria Julian, Rebecca Manners, Cailin Orr, Steve Powers, Hollis Rhinelander, Adam Riggsbee, Daisy Small, Matt Smith, and Sarah Zahn assisted with field and laboratory work. We are grateful to three anonymous reviewers whose comments helped fine-tune the manuscript.

References

Baker, K. S., and R. C. Smith (1979), Quasi-inherent characteristics of the diffuse attenuation coefficient for irradiance, *Soc. Photo-opt. Instrum. Eng.*, *208*, 60–63.

Baron, J. S., et al. (2002), Meeting ecological and societal needs for freshwater, *Ecol. Appl.*, *12*, 1247–1260.

Bott, T. L., et al. (2006), Ecosystem metabolism in Piedmont streams: Reach geomorphology modulates the influence of riparian vegetation, *Ecosystems*, *9*, 398–421.

Brown, J. H., et al. (2004), Toward a metabolic theory of ecology, *Ecology*, *85*, 1771–1789.

Chazdon, R. L., and R. W. Pearcy (1991), The importance of sunflecks for forest understory plants, *BioScience*, *41*, 760–766.

Davies-Colley, R. J. (1987), Optical properties of the Waikato River, New Zealand, *Mitt. Geol.-Paleontol. Inst. Univ. Hamb., SCOPE/UNEP Sonderband*, *64*, 443–460.

Davies-Colley, R. J. (1990), Frequency distributions of visual water clarity in 12 New Zealand rivers, *N. Z. J. Mar. Freshwater Res.*, *24*, 453–460.

Davies-Colley, R. J., and M. E. Close (1990), Water colour and clarity of New Zealand rivers under baseflow conditions, *N. Z. J. Mar. Freshwater Res.*, *24*, 357–365.

Davies-Colley, R. J., and J. W. Nagels (2008), Predicting light penetration into river waters, *J. Geophys. Res.*, doi:10.1029/2008JG000722, in press.

Davies-Colley, R. J., and G. W. Payne (1998), Measuring stream shade, *J. North Am. Benthol. Soc.*, *17*, 250–260.

Davies-Colley, R. J., and J. M. Quinn (1998), Stream lighting in five regions of North Island, New Zealand: Control by channel size and riparian vegetation, *N. Z. J. Mar. Freshwater Res.*, *32*, 591–605.

Davies-Colley, R. J., and J. C. Rutherford (2005), Some approaches for measuring and modelling riparian shade, *Ecol. Eng.*, *24*, 525–530.

Davies-Colley, R. J., et al. (1984), Optical characterisation of natural waters by PAR measurement under changeable light conditions, *N. Z. J. Mar. Freshwater Res.*, *18*, 455–460.

Davies-Colley, R. J., et al. (1992), Effects of clay discharges on streams. part I: Optical properties and epilithon, *Hydrobiologia*, *248*, 215–234.

Davies-Colley, R. J., et al. (2003), *Colour and Clarity of Natural Waters*, 310 pp., Ellis Horwood, New York.

DeNicola, D. M., et al. (1992), Influences of canopy cover on spectral irradiance and periphyton assemblages in a prairie stream, *J. North Am. Benthol. Soc.*, *11*, 391–404.

Doyle, M. W., and E. H. Stanley (2006), Exploring potential spatial-temporal links between fluvial geomorphology and nutrient-periphyton dynamics in streams using simulation models, *Ann. Assoc. Am. Geogr.*, *96*, 687–698.

Evans, G. C., and D. E. Coombe (1959), Hemispherical and woodland canopy photography and the light climate, *J. Ecol.*, *47*, 103–113.

Frazer, G. W., et al. (1999), Gap Light Analyzer (GLA), version 2.0: Imaging software to extract canopy structure and gap light transmission indices from true-colour fisheye photographs, users manual and program documentation, 40 pp., Simon Fraser Univ. and Inst. of Ecosystem Stud., Burnaby, B.C.

Gordon, H. R. (1989), Can the Lambert-Beer law be applied to the diffuse attenuation coefficient of ocean water?, *Limnol. Oceanogr.*, *34*, 1389–1409.

Gordon, N. D., et al. (2004), *Stream Hydrology: An Introduction for Ecologists*, 429 pp., John Wiley, Chichester.

Jerlov, N. G. (1976), *Marine Optics*, 231 pp., Elsevier, Amsterdam.

Julian, J. P., M. W. Doyle, S. M. Powers, E. H. Stanley, and A. Riggsbee (2008), Optical water quality in rivers, *Water Resour. Res.*, doi:10.1029/2007WR006457, in press.

Kelly, D. J., et al. (2003), Effects of solar ultraviolet radiation on stream benthic communities: An intersite comparison, *Ecology*, *84*, 2724–2740.

Kenworthy, S. T., and B. L. Rhoads (1995), Hydrologic control of spatial patterns of suspended sediment concentration at a stream confluence, *J. Hydrol.*, *168*, 251–263.

Kiffney, P. M., et al. (2004), Establishing light as a causal mechanism structuring stream communities in response to experimental manipulation of riparian buffer width, *J. North Am. Benthol. Soc.*, *23*, 542–555.

Kirk, J. T. O. (1994), *Light and Photosynthesis in Aquatic Ecosystems*, 509 pp., Cambridge Univ. Press, New York.

Koch, R. W., et al. (2004), Phytoplankton growth in the Ohio, Cumberland and Tennessee Rivers, USA: Inter-site differences in light and nutrient limitation, *Aquat. Ecol.*, *38*, 17–26.

Leopold, L. B., and T. Maddock Jr. (1953), The hydraulic geometry of stream channels and some physiographic implications, *U.S. Geol. Surv. Prof. Pap.*, *252*, 1–57.

Mobley, C. D. (1994), *Light and Water: Radiative Transfer in Natural Waters*, 592 pp., Elsevier, San Diego, Calif.

Mulholland, P. J., et al. (2001), Inter-biome comparison of factors controlling stream metabolism, *Freshwater Biol.*, *46*, 1503–1517.

Palmroth, S., et al. (2005), Contrasting responses to drought of forest floor CO_2 efflux in a Loblolly pine plantation and a nearby Oak-Hickory forest, *Global Change Biol.*, *11*, 421–434.

Phlips, E. J., et al. (2000), Light availability and variations in phytoplankton standing crops in a nutrient-rich blackwater river, *Limnol. Oceanogr.*, *45*, 916–929.

Poff, N. L., et al. (1997), The natural flow regime, *BioScience*, *47*, 769–784.

U.S. Department of Agriculture (USDA) (2007), UV-B Monitoring and Research Program. (Available at http://uv.ntel.colostate.edu/UVB/)

Scarsbrook, M. R., and J. Halliday (1999), Transition from pasture to native forest land-use along stream continua: Effects on stream ecosystems and implications for restoration, *N. Z. J. Mar. Freshwater Res.*, *33*, 293–310.

Smith, D. G., et al. (1997), Optical characteristics of New Zealand rivers in relation to flow, *J. Am. Water Resour. Assoc.*, *33*, 301–312.

Song, C. H., and L. E. Band (2004), MVP: A model to simulate the spatial patterns of photosynthetically active radiation under discrete forest canopies, *Can. J. For. Res.*, *34*, 1192–1203.

Strayer, D. L., et al. (2006), Using geophysical information to define benthic habitats in a large river, *Freshwater Biol.*, *51*, 25–38.

Taylor, S. L., et al. (2004), Catchment urbanisation and increased benthic algal biomass in streams: Linking mechanisms to management, *Freshwater Biol.*, *49*, 835–851.

Vannote, R. L., et al. (1980), The river continuum concept, *Can. J. Fish. Aquat. Sci.*, *37*, 130–137.

Westlake, D. F. (1966), The light climate for plants in rivers, in *Light as an Ecological Factor*, edited by R. Bainbridge et al., pp. 99–118, Blackwell Sci., Oxford.

Wetzel, R. G. (2001), *Limnology: Lake and River Ecosystems*, 1006 pp., Elsevier, San Diego, Calif.

Yard, M. D., et al. (2005), Influence of topographic complexity on solar insolation estimates for the Colorado River, Grand Canyon, AZ, *Ecol. Modell.*, *183*, 157–172.

Zheng, X., et al. (2002), Variability of the downwelling diffuse attenuation coefficient with consideration of inelastic scattering, *Appl. Opt.*, *41*, 6477–6488.

M. W. Doyle, Department of Geography, University of North Carolina, 205 Saunders Hall, Chapel Hill, NC 27599-3220, USA. (mwdoyle@email.unc.edu)

J. P. Julian, Appalachian Laboratory, University of Maryland Center for Environmental Science, 301 Braddock Road, Frostburg, MD 21532, USA. (jjulian@a1.umces.edu)

E. H. Stanley, Center for Limnology, University of Wisconsin, 680 N. Park Street, Madison, WI 53706, USA. (ehstanley@wise.edu)